Transient Response of Particle Distribution in a Chamber to Transient Particle Injection

Ning Zhang*, Zhongquan Zheng, Steven Eckels**, Venkata B. Nadella**, Xiaoyang Sun****

(Received: 21 September 2008; in revised form: 10 July 2009; accepted: 1 September 2009)

DOI: 10.1002/ppsc.200800043

Abstract

We inject a large number of newly created nano-particle aggregates into a chamber for the purpose of removing harmful contents in an indoor environment. This study is to experimentally and numerically investigate transient response of particle distributions to particle injections. A room-sized chamber of 4 m × 2.1 m × 2.4 m is connected to a specially designed particle-injection system, with two Optical Particle Counters used to simultaneously measure particle-number densities with the size range from 0.3 μm to 10 μm at the inlet and in the chamber. A velocity probe measures the flow that is up to 1 m/s. An Euler-type particulate-phase-transport model is developed and validated by comparing with experimental data. The study shows that the transient behavior of particle distributions is determined by many factors, including particle size, particle settling speed, sampling location, and velocity distribution. Particle number densities decrease in time more quickly for large particles than for small particles, and locations farther downstream in the chamber correlate more weakly with the inlet injection.

Keywords: particle transient measurement, particle transport, simulation, two-phase flow

1 Introduction

Determination of distributions of nano- and micro-sized particles throughout chambers and enclosures with particle injections is very important for many agricultural, industrial and military applications such as indoor air quality, combustion, and species distributions. Most of the studies in a chamber environment with particle injections deal with uniform or steady injections which leads to steady particle-number distribution inside the chamber. Studies of transient injection are scarce, and mostly on liquid injections, e.g. [1]. Particulate transient distributions in fluidized bed with injections were studied by some researchers, e.g. [2], when the injections are flow injections without carrying particles. With transient particle injections, the particle-number distributions inside the chamber are transient as well, and are sensitive to the injections in many cases. The study in this paper aims to a project of using nano-particle aggregates in an injected flow to remove smoke or toxic agents in a room [3]. Flow injection is commonly used among nano-particle delivery methods such as spray or explosion. This type of injected flow is fully transient, and the particle-number density changes rapidly with time. It thus becomes very important to understand the transient response of particle-number distribution inside the room to the injection because it dictates the rate of collisions between nano-particle aggregates and smoke particles, and dictates the effectiveness of smoke reduction and toxin clearing. We have developed a numerical model to simulate this transient smoke reduction process [4]. In this paper, without considering particle collisions, we validate the model's capability of predicting particle transient response to the injection. Because measured data with transient time histories can provide a strict validation for numerical models, the fact that

* Prof. N. Zhang (corresponding author), Department of Engineering, McNeese State University, Lake Charles, Louisiana 70609 (USA).
E-mail: nzhang@mcneese.edu

** Prof. Z. C. Zheng, Prof. S. Eckels, V. B. Nadella, X. Sun, Department of Mechanical and Nuclear Engineering, Kansas State University, Manhattan, Kansas 66506-5205 (USA).

these data are lacking hinders the capability in developing numerical models. In this paper, we describe the experiment that is designed for this kind of measurement.

Reviews of the research on gas-particle flows have been presented in [5, 6]. Numerically, Holmberg and Li [7] defined the requirement for using the Euler-type method for the particulate phase as the particle size must be smaller than the Kolmogorov length scale for turbulent flow. Eulerian approaches were also implemented [8, 9] to simulate the gas-particle flow in ventilated rooms. In both studies, although there was a flow inlet, particles were generated from the floor with a constant production rate. There was no particle injection from the inlet. Kolaitis and Founti [10] performed a transient simulation of particulate material flow in a gravitational classification chamber (GCC) with particle injections using a Lagrangian method. In their study, there was no comparison to experimental data. In fact, because of the nature of the Lagrangian approach, which tracks particle trajectories, a post-process of the computational data, such as statistical averaging, would be needed to provide quantitative information about particle-number density or mass concentration for comparisons.

Experimentally, one of the challenges is how to design a good particle injection system. The problem faced by researchers in this quest is two folds. One is agglomeration of particles that are not within the considered size range. The other is the size distribution. Once agglomerates are broken down, it must be ensured that the sample has the necessary size ranges needed for the experiment. Particle generators previously designed include the brush dispenser and pin mill [11], the mixer type dispenser [12] and the cyclone generator [13]. However for experiments that were done using the chamber, these particle generators were not acceptable due to various constraints like space, power consumption, effectiveness, etc. Therefore a completely new means of particle injection was developed as part of this study.

Optical particle counters (OPCs) are widely used to measure particle size distributions in air. Recent studies include [14, 15, 16]. Most of them measured pollution particles in the outdoor environment. Adachi et al. [17] performed simultaneous measurements of particle size and charge distributions in a clean room. There was no flow physics or transient characteristics of particles presented in their study.

In the present study, a transient particle injection flow in a chamber was studied numerically and experimentally to understand the particle-number distribution in response to the transient injection. Numerically, an unsteady Euler-Eulerian method was used for simulations, i.e. both, the flow and particulate matters are modeled using the Eulerian type of convection-diffusion simulation. Measured transient inlet data were used in simulations as boundary conditions. A particle injection system was designed to overcome some major problems and constraints of experiments performed in a chamber. These problems include: interferences between the injection system and the air flow pattern, influences of injection particles on the air velocity, control of the amount of particles injected, forming of agglomeration, and so on. Because of the transient nature of particle distributions due to transient particle injections, time histories of particle-number densities were measured using two OPCs that enabled simultaneous counts of particles at the inlet duct and a location in the chamber to capture the transient response. This unique two-OPCs setup maximizes the accuracy of comparisons between measured date and simulation results.

2 Experimental Setup

Figure 1 illustrates the chamber geometry with spatial dimensions 4 m × 2.1 m × 2.4 m (13 ft × 7 ft × 8 ft) in x, y and z directions. The overall system is illustrated in Figure 2. The test chamber is under a controlled environment for temperature, humidity and air flow rate during the experiment. Using a DANTEC Mini CTA hot-wire probe, air velocities at different locations in the chamber were measured. The particle injection system is located under the inlet duct of the chamber and connected to the inlet duct with a thin copper tube, so that particles can be entrained in the air flow going into the chamber. Two OPCs were used, which allowed the simultaneous collection of data at the inlet duct and a corresponding position in the chamber for the study of transient behavior of particle-number distribution in the chamber in response to the injection.

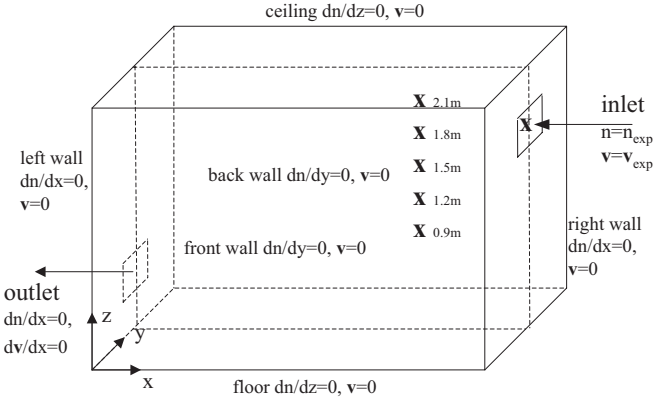

Fig. 1: Illustration of the test chamber, coordinate system and the boundary conditions. Symbol "x" represents the measurement locations.

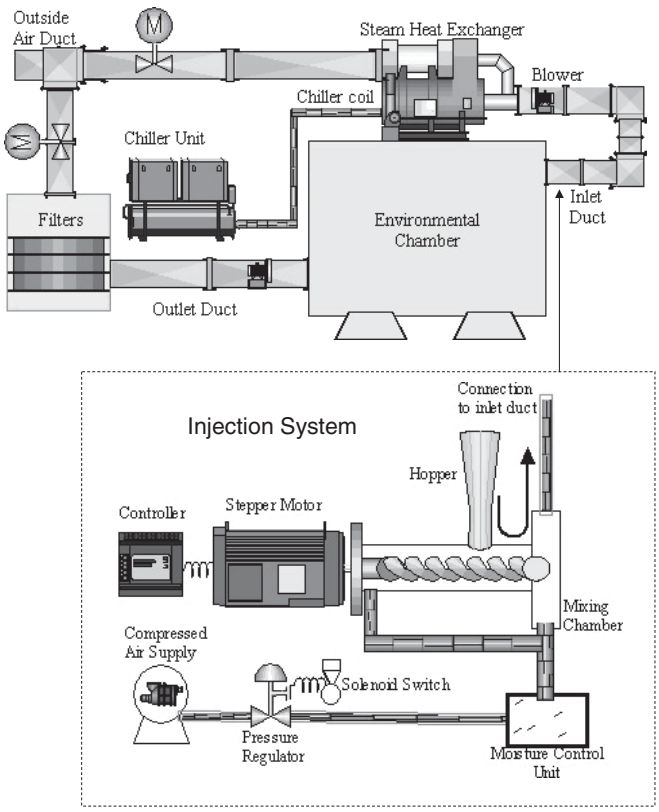

Fig. 2: Illustration of experiment system and particle injection system setups.

The test chamber shown in Figure 1 is made of Plexiglas on all the walls except the floor. The floor is made of wood. It has an inlet duct and an outlet duct, to facilitate the movement of air into and out of the chamber. There is a blower in each duct. The size of both of the inlet and outlet ducts is 0.3 m × 0.3 m (1 ft × 1 ft).

The inlet duct is located 0.3 m from the top of the chamber, while the outlet duct is located 0.3 m from the floor of the chamber, and both are located at the center of the *y* direction. The air coming into the chamber can either be drawn from the outside atmosphere or be recirculated with air coming out from the outlet duct. As air comes out from the chamber, it passes through a series of filters designed to eliminate the particulate matters and dust particles in the air.

A DANTEC model P-16 CTA hotwire probe was used to measure the velocity of air at various points across the inlet duct as well as in the chamber. The uncertainty, which refers to the difference between the actually measured velocity and the calculated velocity, has an averaged value of less than 4 % in the measurement velocity range for this study.

A particle injection system that could be placed outside the chamber was developed so that it would not interfere with air flow patterns. In the present experiment setup, the particle injection system is placed under the inlet duct and connected the inlet duct with a thin copper tube. The construction and operation of the injection system is shown in Figure 2. A National Instruments NI MID 7604/7602 4/2 axis stepper motor is the most essential part of the injection system, and is controlled by a computer to vary the speed. This stepper motor is connected to a long lead screw encased in a plastic tube. A hopper is attached to the top of the casing, to feed particles into the lead screw. The hopper has a valve through which the amount of particles being dumped onto the lead screw can be controlled. Due to air flowing into the chamber, particles are thoroughly mixed and agglomeration is avoided. There is a thin copper tube connecting the mixing chamber to the inlet duct of the chamber. The compressed air that mixes particles also drives them through the copper tube and into the inlet duct, thereby allowing for the injection of particles into the chamber. The amount of compressed air being sent into the mixing chamber is controlled by a pressure regulator, set up underneath the stepper motor. Usually the pressure of air is set to 34.5 Kpa (5 psi). This pressure does not significantly affect the velocity of air going into the chamber. A moisture control unit is also connected to the pressure regulator to ensure that air being sent into the chamber is relatively dry and free of moisture. A pressure balancing technique is used to ensure that particles do not push back the lead screw due to the pressure in the mixing chamber.

In the experiment, PECTRO.3 version OPCs by CLIMET were used. The particle counter gave counts in 16 channels, varying from 0.3 μm to 10 μm. Since the OPC could not be positioned accurately at some points in the chamber, a nozzle and plastic tube were used to take measurements at all points. The nozzle was placed at the point of measurement and a plastic tube connected the other end of the nozzle to the probe on top of the OPC. The diameter of the nozzle is about 6.5 mm. The OPC was set to draw in air at the rate of 4.72×10^{-6} m^3/s (0.01 cfm). The sampling nozzle was selected to ensure iso-kinetic sampling of air in the chamber. Because the objective was to study the transient behavior of particle-number distributions inside the chamber in response to the inlet, two OPCs were used in the experiment; one for the inlet and the other for a location inside the chamber, shown in Figure 1. Since two different OPCs were used, a calibration process was required to ensure that the reading given by both were consistent.

In the test chamber, the temperature was set to 21 °C (70 °F); the relative humidity was set to 0 %. Using fans, the flow rate was set to 0.189 m^3/s (400 cfm). After velocity measurements, OPCs were switched on and initial data were collected. Following that, particles were fed through the inlet duct and both OPCs started taking

transient data. It needs to be mentioned that the readings from inlet OPC show that particle-number-density value is always higher at the first several minutes of the injection. After that period, it decreases significantly to a smaller but stable value. This unsteady feature is unavoidably caused by the injection system; however, it represents the actual transient feature of the nano-particle injection in the smoke-reduction application [3]. The response of particle-number distribution inside the chamber to this transient injection needs to be studied. For every experiment, about 40 grams of spherical glass particles were used.

The optical particle counters were calibrated as a pair to ensure that the readings corresponded during transient measurement. Due to the irregular optical shape of the particles, some deviations from ideal were expected. Five calibration runs were performed with both optical counters reading at the same location in the chamber. After calibration, the average reading and 95 % confidence intervals were compared, and it was found that OPC agreed within ± 6 % at the low particle sizes and within ± 10 % at the larger sizes.

3 Model Description

The air/solid-particle flow problem is simulated by using an Euler-type formulation for both air flow and particulate phase. In this work, only the particle-number concentration is the concern for the particulate phase. Therefore, the Euler-type simulation is suitable, instead of the Lagrange-type simulation that is for motions of individual particles.

3.1 Fluid Flow Phase Model

The continuous air-flow phase is governed by unsteady incompressible flow equations

$$\vec{\nabla} \cdot \vec{u} = 0 \tag{1}$$

and

$$\rho \frac{D\vec{u}}{Dt} = -\vec{\nabla} p + \vec{\nabla} \cdot \bar{\bar{\tau}}, \tag{2}$$

where ρ, $\vec{u}$, p, and $\bar{\bar{\tau}}$ are the flow density, velocity, pressure, and viscous shear stress, respectively. The body force, either due to the gravitational acceleration or arising from interactions with solid particles, is neglected because of small particle sizes and, more importantly, light-loading of particulate phase considered in this study. For the problems considered in this study, the Kolmogorov length scale in turbulent flow is relatively large in comparison to particle sizes, a fact to be shown in the later section. This justifies the assumption that particles do not create a significant wake and do not enhance turbulence, and instead they add to the dissipation that depends on the mass loading. In addition, with the light-loading particulate phase [18] considered here, we can thus assume that the air flow affects the particulate phase significantly, while the behavior of the particulate phase does not impose any effect on the air flow.

3.2 Particulate Phase Model

The particulate-phase transport equation includes effects of flow convection, both, laminar and turbulent diffusion, and settling velocity of the particle. It needs to be noted that the settling velocity is in the z-direction in the current coordinate system, and can be combined with the convection term. All other effects are neglected in this study. The equation is

$$\frac{\partial n_i}{\partial t} + \vec{\nabla} \cdot \left[n_i \left(\vec{u} + \vec{U}_{sett} \right) \right] = \vec{\nabla} \cdot \left(D_i \vec{\nabla} n_i \right), \tag{3}$$

where n_i and D_i are the particle-number density (count/volume) and the diffusion coefficient (both, laminar and turbulent) of the i-size particles in the air, and $\vec{U}_{sett}$ is the particle settling speed, defined as:

$$\vec{U}_{sett} = C_c \tau_p \vec{g}. \tag{4}$$

In Eq. (4), C_c is the slip correction factor [19], $\vec{g}$ is the gravitational acceleration, and τ_p is the particle response time defined as:

$$\tau_p = \frac{\rho_p d_p^2}{18\mu}.$$

The diffusion coefficient, D_i, is calculated as

$$D_i = D_m + D_t, \tag{5}$$

where D_m is the molecular diffusion coefficient and D_t is the turbulent diffusion coefficient. Following the Stokes-Einstein expression, we have [19]:

$$D_m = C \frac{\kappa T}{3\pi\mu d_p}, \tag{6}$$

where $\kappa = 1.38 \times 10^{-23}\, Nm/K$ is the Boltzmann constant, T is the temperature, and C is Cunningham's correction factor and is 1.0 for the size range of particles in this

study [19]. The turbulent diffusion coefficient, D_t, is related to the turbulent eddy viscosity of the flow with

$$D_t = \frac{\mu_t}{\rho Sc_t}, \tag{7}$$

where μ_t and Sc_t are the turbulent viscosity and turbulent Schmidt number, respectively. The Schmidt number measures the relative diffusion of momentum and mass due to turbulence and is on the order of unity in all turbulent flows. It is an empirical constant that is relatively insensitive to molecular fluid properties. Since particle sizes are smaller than the Kolmogorov length scale in this study as stated previously, particles mainly follow turbulent eddies. Here Sc_t is set to be 0.7 for all cases, based on Yimer et al.'s [20] observation for simulations of turbulent free jet. The laminar diffusion coefficient is a constant in the range of certain particle sizes, and it is in the order of 10^{-10}, such that it is much smaller than the turbulent diffusion coefficients in most of the computational domain. However, since there are several very small turbulence diffusion coefficient values (close to zero) on locations near the walls because of the small turbulence viscosity there, the laminar diffusion coefficient is not neglected in the simulation.

While Eq. (3) applies to any *i*-size particles and coagulations between different sizes of particles are neglected, the subscript *i* is omitted for simplicity in the following discussion.

3.3 Solution Procedures

In the solution procedure, the FLUENT flow solver with the RNG k-ε turbulence model is used to solve Eqs. (1) and (2). The computational scheme is second-order in time and space. The second-order upwind scheme is used for convection terms, and the second-order central differencing is used for diffusion terms. In particulate-phase computing subroutines, the same computational scheme as the flow solver is used to solve Eq. (3). For boundary conditions of particulate phase, shown in Figure 1, the normal derivatives of the particle-number density are set to be zero on the walls and at the outlet. Specifying zero normal derivatives on the walls is a physically realistic way to indicate that there is no diffusion-caused surface deposition on the walls for the sizes of particles considered in this study. The zero normal derivative at the outlet is a simplified outflow condition for the particle-number density. At the inlet, values of n are specified.

It is not trivial to implement the solution algorithm of a passive scalar transport equation to solve Eq. (3), and readers are referred to a previous publication for the detailed implementation [4]. Here we need to point out specific issues about inlet boundary conditions and transient inlet measurement data. In the simulation, the time histories of measurement data at the inlet need to be input into the solver as the inlet boundary conditions. Because the number of measurement points on the inlet surface is less than the number of grid points in the simulation, and also because the measurement time interval is larger than that used in the simulation, both, spatial and temporal interpolations are required. It needs to be noted that the swirling effect in the inlet flow is not considered in the inlet boundary condition of the current numerical model. It was expected that the injection device was designed such that the swirling effect was negligible, at least at the inlet of the chamber. However, some of the discrepancies between the measured data and the simulated results could be due to this assumption.

Another issue is the boundary condition due to the settling velocity effect. One thing peculiar about the settling velocity is that although it is a property of particles, from Eq. (3) it is treated as part of the background velocity to the particulate phases in the current computational scheme. Therefore, it requires boundary conditions. From integrating Eq. (3) within the chamber volume we obtain that the change of total particle number in the chamber is determined by the deposition rate, $U_{sett}\, n$, on top and bottom surfaces. If $U_{sett} = 0$ on both of top and bottom wall boundaries, there is no change of the total particle number. In order to include the fact that the number of particles is reduced due to settling, the bottom wall boundary needs to be assumed "leaking," i.e., the settling velocity at the bottom wall boundary is the same positive constant value as that in the field. Then the total particle number decreases because of the settling effect. The assumption of $U_{sett} = 0$ at top wall ensures that no particle "leaks" into the chamber through the ceiling from outside. The validation of this settling treatment with analytical solution and details of modeling the settling effect with inlet and outlet were presented in a previous publication [21].

4 Results and Discussions

Since velocity is relatively steady and does not change with time, we can measure at many locations across the inlet surface as well as inside the chamber separately. However, due to the transient nature of the particulate phase, we have to measure the particle-number densities at inlet and a location inside the chamber simultaneously. One of the OPCs is thus placed at the center of the inlet surface. One concern is that the inlet distribution is not uniform, thus the center value is not a repre-

sentation of the whole area. Therefore before the measurement inside the chamber, we used both OPCs to determine the inlet distribution. We used the measured inlet data to determine a pattern of inlet particle-number distribution calibrated to the center particle-number density value. We repeated the whole process several times and found the pattern is consistent and does not change significantly over time. Then during the experiments, with the knowledge of the particle-number density at the center of the inlet surface, the inlet particle-number distribution on the whole surface can thus be obtained using the pre-determined pattern. The inlet distribution determined in this way can be used as input to simulations as inlet boundary conditions.

In the simulation, the velocity field was calculated without the particles and compared with measurement data in advance to ensure an accurate flow field used for particulate-phase study. The pre-calculated velocity field is then treated as background velocity field for the particulate phase simulation. This is justified by the one-way flow/particle interaction assumption. From the simulation result, the minimum Kolmogorov length scale in the chamber is 163 μm, which is much larger than the particle size we consider. Therefore, the Euler-type particulate phase model can be used. Time histories of particle-number densities at different locations inside the chamber were recorded during the simulation for comparisons with measured data. A computational grid mesh of $120 \times 68 \times 74$ is placed in x, y and z dimensions, and 10×10 at both, inlet and outlet. Higher resolution grids ($240 \times 136 \times 148$ and 20×20) were also tested, and the results of the two grid resolutions agree well with each other. This means the $120 \times 68 \times 74$ grid mesh used in the computation is sufficient for achieving grid-independent simulation results.

4.1 Velocity Comparisons

Velocity measurements are taken at several points across the cross section of the inlet duct. Since the inlet duct is square, it is divided into 9×9 grid along which the measurements are taken. The hotwire probe was mounted on a probe rotator. Using the rotator, both, the horizontal angle as well as the vertical angle of the hotwire can be changed. The measurement shows that the flow going out of the inlet has a 10° downward inclinative angle. Along with velocities at the inlet duct, measurements were also done along the y-directional vertical central cutting plane of the chamber. There are 56 measurement points (7×8, 7 in the x direction) evenly distributed on the measurement plane.

In the simulation, measured velocity values on the inlet duct surface are interpolated into 10×10 grid mesh. The 10° downward direction of the inlet flow is also specified. The inlet turbulent intensity is set to be 20 %, based on the measurement data. The velocity field is steady. The averaged inlet velocity is about 2 m/s, resulting in the Reynolds number based on the size of the inlet duct about 40,000. Figure 3 compares the velocity magnitude profile along the vertical (z) direction in the center of the chamber. In this figure, shapes of both profiles agree well, and both peak locations match exactly at 1.7 m and 0.15 m above the floor which correspond to heights of the inlet and outlet duct. However, the simulation result under-predicts a little for the peak value. On y-directional central cutting plane, we also look at the maximum velocity locations and values between the measured date and simulation results and there is a good agreement. It is evident that the velocity continues to decrease along the injection trajectory. It can be concluded that overall agreements between experimental data and simulation results for the velocity field are reasonably good.

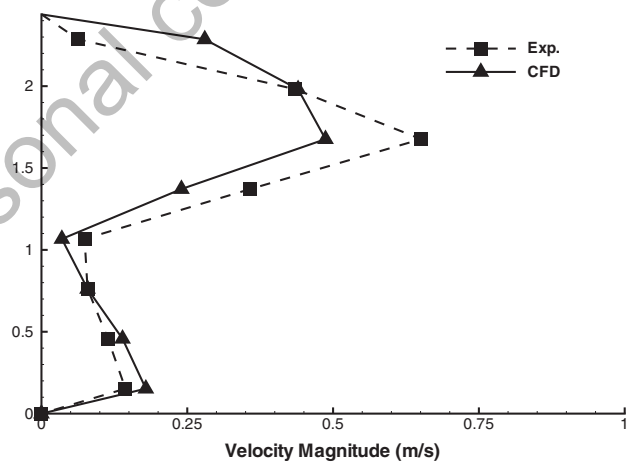

Fig. 3: Variation of velocity magnitude with vertical locations at the center of the chamber.

4.2 Steady State Cases

Once the velocity measurements were done and the air flow patterns in the test chamber were mapped, it was ready to inject particles. For all cases in this paper, particle-number densities in the chamber were measured using one OPC at different locations on a vertical (z-direction) line in y-directional centre-cutting plane of the chamber, and a quarter of the chamber length away from the inlet duct. And the measurement locations are 0.9, 1.2, 1.5, 1.8 and 2.1 m (3, 4, 5, 6 and 7 ft) from the floor, shown in Figure 1. Since there was only one OPC for measurements inside the chamber, five experiments were needed to get particle-number-density values on

all five locations. Since the inlet conditions were not the same at different experiments, we needed the other OPC to collect inlet data all the time. Particle sizes are grouped into six size ranges. Table 1 shows characteristic diameters and settling velocities of these size ranges. In the simulation, these six sizes are treated as six independent particulate phases and Eq. (3) is computed separately for each of them.

Table 1: Particle size and setting velocity.

charateristic size (μm)	size range (μm)	settling velocity (m/s)
1	0.7-1.3	0.0000304
1.75	1.3 - 2.2	0.00009309
3.1	2.2 - 4	0.0002921
4.75	4-5.5	0.0006858
6.25	5.5-7	0.0011873
8.5	7-10	0.002196

In a previous publication [22], results of this computational model were compared with experiment data from Wang et al. [23] under a steady-state condition, and the agreement was good. Here we want to validate the steady-state simulation again in this particular test chamber. The sampling time interval in steady cases is 5 min, thus the collected data are not sensitive to time and represent the overall characteristics of particle distributions. It was observed that from 15 min to 45 min, the counts of particles were relatively stable. Therefore, counts of particles within the 15–45 min interval are taken as the standard counts and used as the steady inlet boundary conditions for the simulation. The time step used in particulate phase simulations is 1 s. The accuracy of the selected time step has been tested by comparing results using a time step of 0.5 s and showing negligible differences.

Figure 4 shows comparisons between experimental and simulation results at two different locations, 1.8 m and 0.9 m above the ground, as shown in Figure 1. The *x*-axes of the plots denote the size ranges and the *y*-axes denote the particle-number densities. Comparisons in Figure 4 show good agreements between experimental and simulation results, and the trend is similar at different heights at which the measurements are taken. The particle size with the most particle number is 3.1 μm, while the largest size, 8.5 μm, has the least number. The simulation results tend to under-predict for the larger sizes and over-predict for the smaller sizes. Simulation results at the location 1.8 m above the ground match the experimental data better, because it is close to the inlet duct where strong flow field and large number of particles are located.

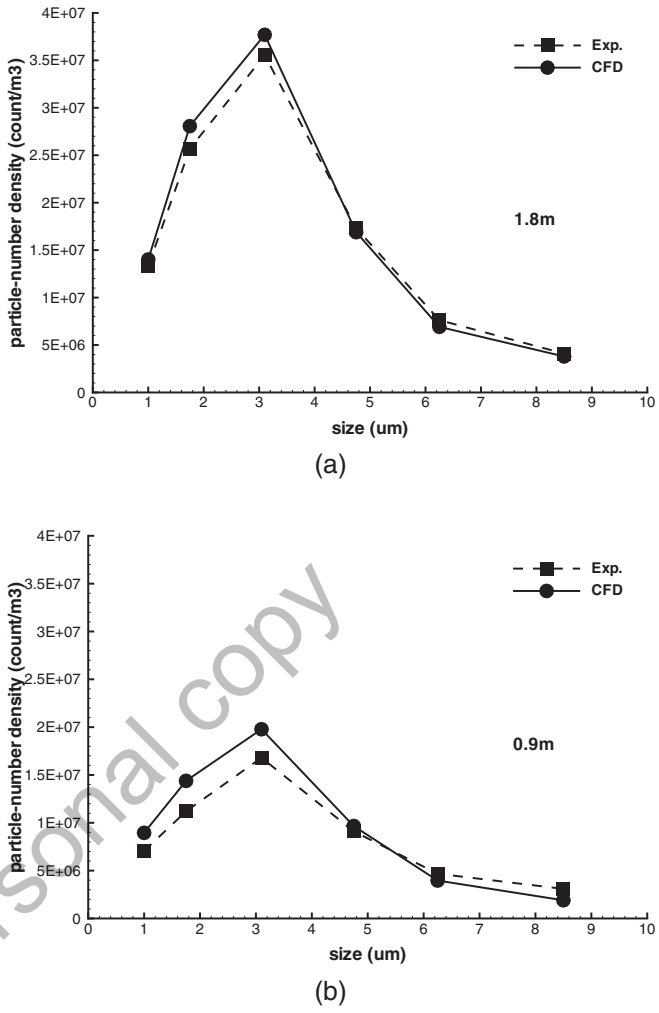

Fig. 4: Variation of particle-number density with particle sizes at different vertical locations for the steady cases. (a) 1.8 m, (b) 0.9 m.

4.3 Transient Particle-Number Density Results

In the transient experiments, the sampling time interval of both OPCs was decreased to 21 s. All other experiment setups were exactly the same as the steady experiments. It needs to be emphasized that one OPC was always placed at the center of inlet duct to record time history of particle-number density. The inlet surface distribution at each sampling time is thus calculated using the measured center value and the pre-determined pattern mentioned in section 3.3. Transient inlet particle-number-density distributions from measurements are then input into the solver as the transient boundary conditions. It needs to be noted that because the measurement time interval is larger than the time step used in the simulation (1 s), a linear interpolation is used to calculate inlet distributions at every time step. The mea-

surements were taken on the same locations inside the chamber as in the steady state cases. The particle-number-density histories were recorded at those target locations during the simulations. The same transient measurements were performed twice to test the consistency of the experiments. Accordingly, two sets of simulations were also performed based on different inlet measurement data. The two sets of results are similar, indicating good consistency and repeatability. For the visual quality of the figures, we present one set of comparisons between experimental and simulation results.

Figures 5–7 are time-history comparisons of particle-number densities of 1 μm, 3.1 μm and 8.5 μm particles

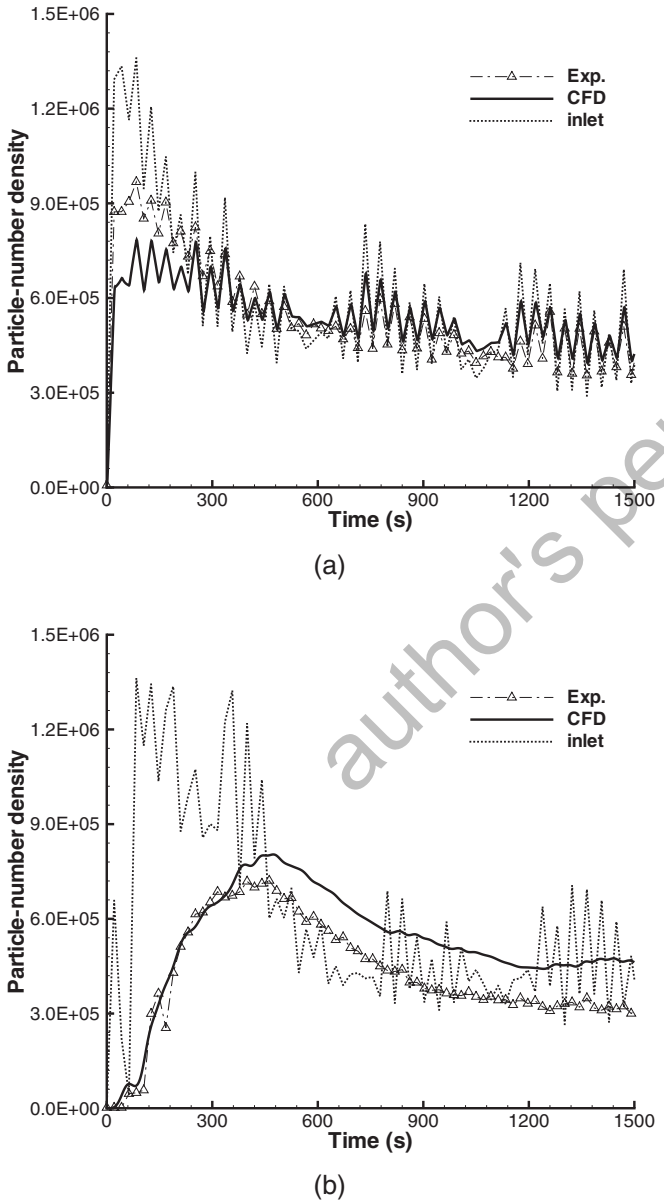

Fig. 5: Time history comparison of particle-number density at two locations for 1 μm particles. (a) 1.8 m, (b) 0.9 m.

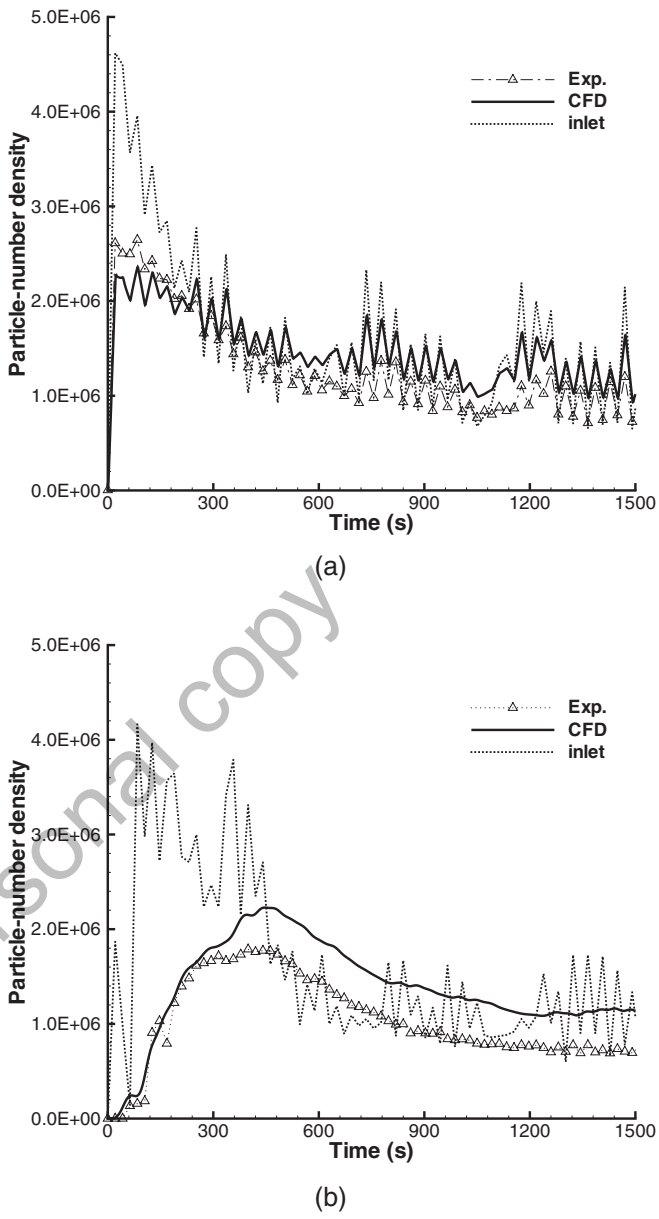

Fig. 6: Time history comparison of particle-number density at two locations for 3.1 μm particles. (a) 1.8 m, (b) 0.9 m.

at 1.8 m and 0.9 m locations. There is an additional curve in each of Figures 5–7, the history of the inlet data. The experiment and simulation share the same inlet history. The reason we provide the inlet data is to show the change of particle-number distribution from inlet, which is an indication of transient response. Note that in all the time-history figures, sharp changes in inlet particle-number density with time throughout tests are caused by the operation of the injection system. For the inlet data, there is a peak of particle-number density at the early stage. After that period, the particle-number density decreases significantly and reaches to a smaller but stable value. This transient injection feature is

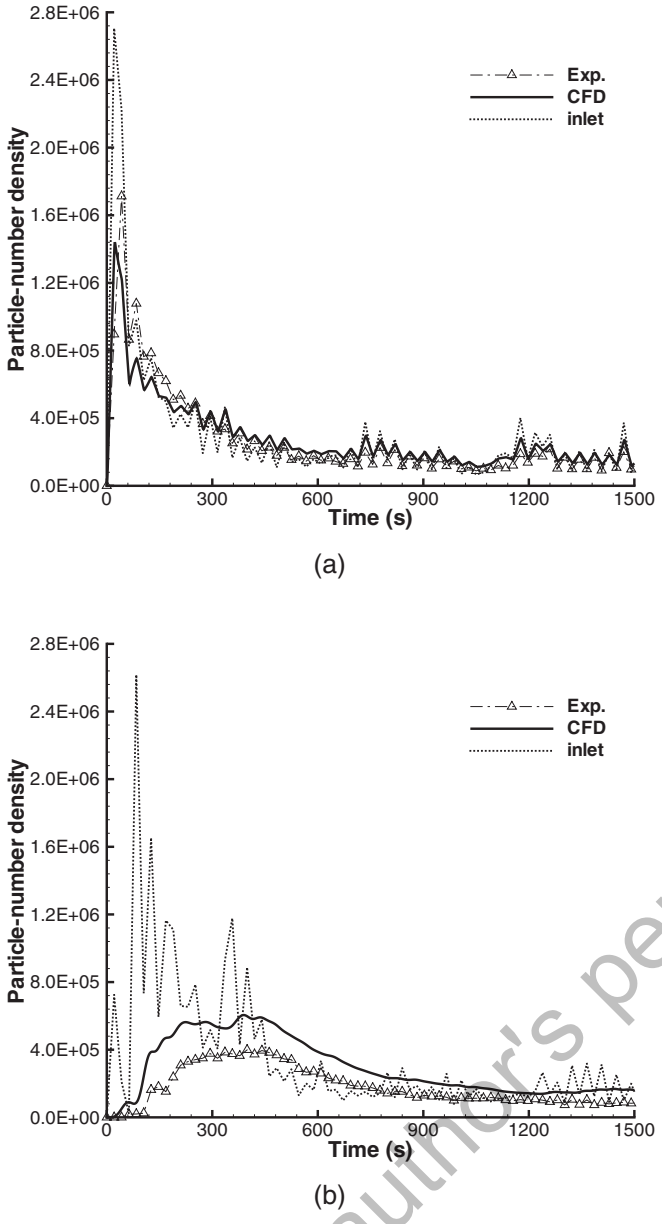

Fig. 7: Time history comparison of particle-number density at two locations for 8.5 μm particles. (a) 1.8 m, (b) 0.9 m.

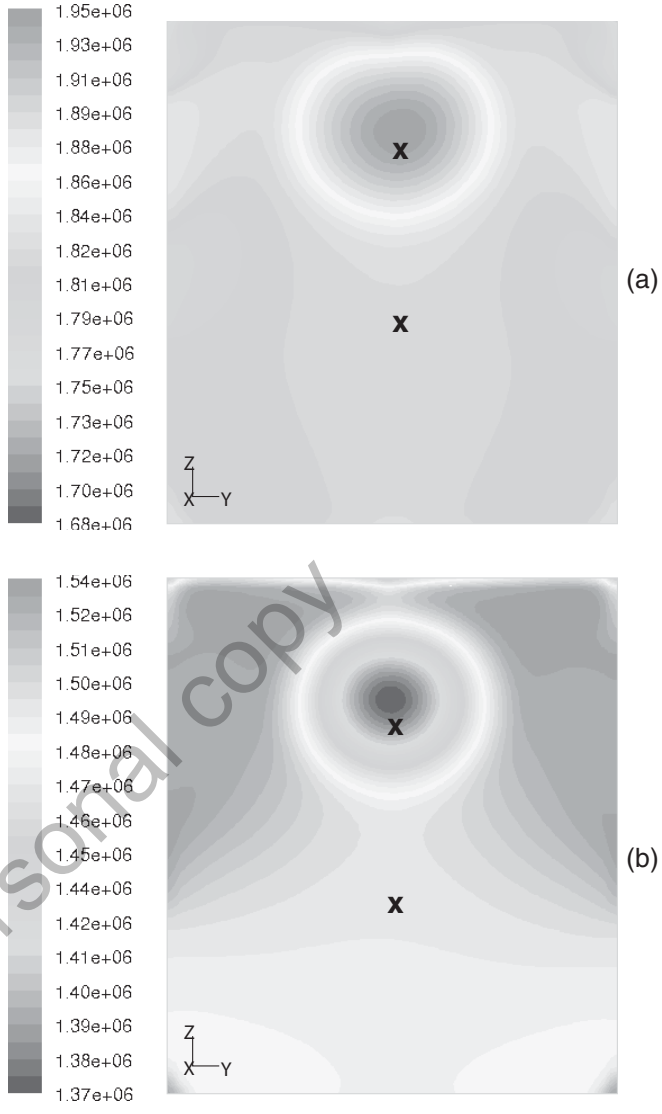

Fig. 8: Particle-number density contours for 3.1 μm particles on measurement *y*-*z* plane at time (a) 300 s, (b) 600 s. Symbol "x" represents the 1.8 m and 0.9 m measurement locations.

reflected in the particle-number distributions inside the chamber. At different locations and for different particle sizes, the responses are different.

The particle-number density values for all different sizes and at all different locations have a common character of a peak value responding to the inlet peak value. At different locations, some differences in response can be found. At 1.8 m location which is the location close to the inlet, the shape of the peak is close to the inlet peak and no delay of peak is found. This indicates a strong response to the injection. However, at 0.9 m location, the peak is clearly smoothed out from the inlet peak and is delayed in time, which shows a weaker response. This can also be found in the contour plots. Figure 8 is the particle-number-density contours for 3.1 μm particles, on the measurement *y*-*z* plane, at two different time. The symbol "x" represents the 1.8 m and 0.9 m measurement locations. At 300 s, when the inlet particle-number density is high, the value at 1.8 m is higher than that at 0.9 m. At 600 s, the inlet value decreases, thus the value at 1.8 m responds to the inlet value quickly and is lower than that at 0.9 m. This clearly indicates a weaker and slower response at 0.9 m than at 1.8 m. It can be concluded that strong responses to the transient injection occur at the locations close to the inlet while weaker responses occur at farther locations. This is because the flow is getting weaker when it is farther away from the inlet, where less convection leads to a rela-

tively more diffusion and settling dominant situation that damps the transient injection effect.

Comparing among different particle sizes, we can also find some different responses. First, the time duration of the peak period is shortened when the particle size increases. Second, the drop from the maximum peak is more significant for large particles than small particles. Both are due to the settling effect. With a higher settling speed, large particles drop to the floor faster than small particles, and more counts of large particles from the injection are deposited to the bottom floor than small ones resulting in a smaller amount of large particles left in the chamber at the end of the transient period.

Comparing with the experimental data, the simulation results also capture those transient features mentioned above with good overall agreements. Simulations and experiments agree the best at the location closest to the inlet duct, 1.8 m, for all particle sizes. It is because, while close to inlet, flow is strong and convection is dominant so that errors caused by other factors are relatively small. There are two aspects for comparison in Figures 5–7, different particle sizes and different sample locations. It is important to quantitatively understand how well the model predicts according to these two aspects. A parameter, named comparison factor, is defined as the ratio between the time averaged simulation data and experimental data. Comparison factor of one indicates a perfect match between the simulation and experimental data, while greater than on means over-predictions from simulation results, and under-predictions otherwise. The comparison factors are calculated for every size at every location (listed in Table 2). From this table, for most of the cases except one, the simulation results over-predict. One possible reason is the under-prediction of the velocity field by the model. For each size of particles, simulation results at 1.8 m agree better with the experimental data than at 0.9 m. For both locations, the comparison factors increase as particle size increases, except for 1.75 μm and 8.5 μm particles. This trend indicates that the current model works better for smaller particles. One reason can be the small-particle-size requirement of the Euler-type particulate-phase model. In the current study, although all particle sizes meet the requirement, the use of smaller particles may yield better numerical solutions.

Table 2: Comparison factors for different locations and particle sizes.

	3ft	6ft
1 μm	1.2532	1.0204
1.75 μm	1.1924	0.9744
3.1 μm	1.3607	1.1886
4.75 μm	1.5808	1.3070
6.25 μm	2.0892	1.7910
8.5 μm	1.6868	1.0946

5 Conclusion

The numerical and experimental studies have been performed for the gas/particle two-phase flow in a test chamber with particle injections. Simulation results of flow and particulate phases have been compared with measurement data. Transient particle-number distributions in response to the injections were studied.

The particles were deployed into the chamber by an injection system specifically designed for this purpose. The two-OPCs setup enables the capture of the transient response experimentally. The velocity field and steady cases were validated in advance to ensure the accuracy of transient studies. The transient results show:

1) An early peak in the inlet particle-number density history shows the transient feature generated by the current injection system.

2) Responses to such a transient injection vary with particle sizes in the injection system: the peak period is shortened as particle size increases; the drop from the peak value is more significant for large particles than for small particles.

3) Responses to the transient injection vary at different downstream locations from the injection: strong responses at the locations close to the injection; at farther locations, the signals are altered, indicating weaker responses. The computational model correctly captures these variations, which warrants the validity of the current model for use in transient simulation.

The overall agreements between experimental and simulation results are good, especially for the response to the transient injection feature. In most of the cases, the simulations over-predict the particle-number densities. We suspect that the slight under-prediction of the velocity field be a possible reason. The mismatch of particle-number densities between the simulation and experiment is smaller at the locations closer to the injection. The error also increases when the particle size increases. One reason could be due to the small-particle-size requirement of the Euler-type particulate phase model. The simulation model has demonstrated the ability to simulate transient gas/particle two-phase flow problems.

6 Acknowledgment

This work was partially funded with a subcontract to Kansas State University from the United Stated Marine Corps Systems Command through M2 Technologies Inc. The first author would also like to acknowledge the sup-

port from Institute for Environmental Research at Kansas State University when he was a Research Associate there.

7 References

[1] L. Allocca, G. Valentino, Droplet Size and Velocity Distributions of a Transient Hollow-Cone Spray for GDI Engines. *Part. Part. Syst. Charact.* **2001**, *18*, 262–270.

[2] Y. Q. Feng, A. B. Yu, Microdynamic Modelling and Analysis of the Mixing and Segregation of Binary Mixture of Particles in Gas Fluidization. *Chem. Eng. Sci.* **2007**, *62*, 256–268.

[3] N. Zhang, Z. C. Zheng, R. G. Maghirang, Numerical Simulation of Smoke Clearing with Nanoparticle Aggregates. *Int. J. Numer. Meth. Eng.* **2008**, *74*, 601–618.

[4] N. Zhang, Z. C. Zheng, A Collision Model for a Large Number of Particles with Significantly Different Sizes. *J. Phys Appl. Phys.* **2007**, *40*, 2603–2612.

[5] D. E. Stock, Particle Dispersion in Flowing Gases. *J. Fluid Eng.* **1996**, *118*, 4 –17.

[6] L. Zhou, *Theory and Numerical Modeling of Turbulent Gas-Particle Flows and Combustion*. Science Press, Beijing and CRC Press, Boca Raton, FL, **1993**.

[7] S. Holmberg, Y. Li, Modelling of the Indoor Environment – Particle Dispersion and Deposition. *Indoor Air* **1998**, *8*, 113–122.

[8] B. Zhao, X. Li, Z. Zhang, Numerical Study of Particle Deposition in Two Differently Ventilated Rooms. *Indoor Built Environ.* **2004**, *13*, 443–451.

[9] M. C. Puma, R. G. Maghirang, M. H. Hosni, L. J. Hagen, Modeling Dust Concentration Distribution in a Swine House under Isothermal Conditions. *Transactions of ASAE* **1999**, *42*, 1811–1821.

[10] D. I. Kolaitis, M. A. Founti, Modeling of the Gas-Particle Flow in Industrial Classification Chambers for Design Optimization. *Powder Technol.* **2002**, *125*, 298–305.

[11] K. Leschonski, B. Benker, U. Bauer, Dry Mechanical Dispersion of Submicron Particles. *Part. Part. Syst. Charact.* **1995**, *12*, 295–298.

[12] H. Masuda, K. Gotoh, Dry Dispersion of Fine Particles. *Colloid Surf.* **1995**, *109*, 29–37.

[13] H. Yoshida, Three Dimensional Simulation of Air Cyclone and Particle Separation by a Revised-Type Cyclone. *Colloid Surf.* **1996**, *109*, 1–12.

[14] M. J. Kleeman, J. J. Schauer, G. R. Cass, Size and Composition Distribution of Fine Particulate Matter Emitted from Motor Vehicles. *Environ. Sci. Tech.* **2000**, *34*, 1132–1142.

[15] J. L. Hand, S. M. Kreidenweis, N. Kreisberg, S. Hering, M. Stolzenburg, W. Dick, P. H. McMurry, Comparisons of Aerosol Properties Measured by Impactors and Light Scattering from Individual Particles: Refractive Index, Number and Volume Concentrations, and Size Distributions. *Atmos. Environ.* **2002**, *36*, 1853–1861.

[16] K. Okada, J. Heintzenberg, Size Distribution, State of Mixture and Morphology of Urban Aerosol Particles at Given Electrical Mobilities. *J. Aerosol Sci.* **2003**, *34*, 1539–1553.

[17] M. Adachi, B. Y. H. Liu, D. Y. H. Pui, Development of an Automatic System for Measuring Particle Charge and Size Distributions in a Clean Room. *Part. Part. Syst. Charact.* **1991**, *8*, 200–208.

[18] N. Zhang, Z. C. Zheng, L. Glasgow, B. Braley, Particle Deposition in a Room-Sized Chamber with Particle Injection. *Proc. ASME Fluid Eng. Division Summer Conf.*, Houston, USA, **2005**.

[19] W. C. Hinds, *Aerosol Techology*. John Wiley & Sons, New York, NY, **1982**.

[20] I. Yimer, I. Campbell, L.-Y. Jiang, Estimation of the Turbulent Schmidt Number From Experimental Profiles of Axial Velocity and Concentration for High-Reynolds-Number Jet Flows. *Can. Aeronaut. Space J.* **2002**, *48*, 195–200.

[21] Z. C. Zheng, N. Zhang, Integral Characteristics of Mass Conservation of Particles in Flow. *Proc. of 4th AIAA Theoretical Fluid Mechanics Meeting*, Toronto, Canada, **2005**.

[22] Z. C. Zheng, N. Zhang, S. Eckels, Validations of Particle/Fluid Interaction Models. *Proc. Intern. Mech. Eng. Congr. Exposition*, Anaheim, CA, USA, **2004**.

[23] X. Wang, Y. Zhang, L. Y. Zhao, G. L. Riskowski, Effect of Ventilation Rate on Dust Spatial Distribution in a Mechanically Ventilated Airspace. *Transactions of ASAE* **2002**, *43*, 1877–1884.

